

# Reprocessed emission from warped accretion discs induced by the Bardeen-Petterson effect

Sheng-Miao Wu<sup>1\*</sup>, Lei Chen<sup>1,2</sup> † and Feng Yuan<sup>1</sup> ‡

<sup>1</sup>*Key Laboratory for Research in Galaxies and Cosmology, Shanghai Astronomical Observatory, Chinese Academy of Sciences, 80 Nandan Road, Shanghai 200030, China*

<sup>2</sup>*Max-Planck-Institut fuer Radioastronomie, Auf dem Huegel 69, 53121 Bonn, Germany*

15 November 2018

## ABSTRACT

The broad Balmer emission-line profiles resulting from the reprocessing of UV/X-ray radiation from a warped accretion disc induced by the Bardeen-Petterson effect are studied. We adopt a thin warped disc geometry and a central ring-like illuminating source in our model. We compute the steady-state shape of the warped disc numerically, and then use it in the calculation of the line profile. We find that, from the outer radius to the inner radius of the disc, the warp is twisted by an angle  $\sim \pi$  before being flattened efficiently into the equatorial plane. The profiles obtained depend weakly on the illuminating source radius in the range from  $3r_g$  to  $10r_g$ , but depend strongly on this radius when it approaches the marginally stable orbit of an extreme Kerr black hole. Double- or triplet-peaked line profiles are present in most cases when the illuminating source radius is low. The triplet-peaked line profiles observed from the Sloan Digital Sky Survey may be a “signature” of a warped disc.

**Key words:** accretion, accretion discs — black hole physics — galaxies: active — line: profiles

## 1 INTRODUCTION

A small fraction of active galactic nuclei (AGNs) with broad lines show double-peaked emission-line profiles, which suggests an accretion disc origin (Eracleous & Halpern 1994, 2003; Strateva et al. 2003; Gezari, Halpern & Eracleous 2007). In a stationary circular relativistic disc model, Doppler boosting will make the blue peak of the profile higher than the red one. However, observations of the variability of line emission in some objects show that at least at some epochs the profile asymmetry is reversed, with the red peak higher than the blue one, contrary to the predictions of homogeneous, circular relativistic disc models (Miller & Peterson 1990; Strateva et al. 2003; Gezari et al. 2007). To adjust the theoretical to the observed profiles, non-axisymmetric or warped discs are usually required. Various physically plausible processes in the accretion flow have been considered, such as spiral shocks, eccentric discs, bipolar outflows or a binary black hole system (Chakrabarti & Wiita 1994; Eracleous et al. 1995; Storchi-Bergmann et al. 1997; Zheng, Sulentic & Binette 1990; Veilleux & Zheng

1991; Begelman, Blandford & Rees 1980; Gaskell 1996; Zhang, Dultzin-Hacyan & Wang 2007b), as well as a warped accretion disc (Wu, Wang & Dong 2008). This warped disc makes it possible for the radiation from the inner disc to reach the outer parts, enhancing the reprocessing emission lines. Thus, warping can both provide the asymmetry required for the variations of the emission lines and naturally solve the long-standing energy-budget problem, because the subtending angle of the outer disc portion to the inner one is increased by the warp.

There are strong observational and theoretical grounds for believing that accretion discs around black holes may be warped and twisted. Evidence for the existence of warped discs in astrophysical systems has been found from observations (Herrnstein et al. 2005; Caproni, Abraham & Mosquera Cuesta 2006; Caproni et al. 2007; Martin, Tout & Pringle 2008). From a theoretical point of view, four main mechanisms for exciting/maintaining warping in accretion discs have been proposed, namely warping that is tidally induced by a companion in a binary system (Terquem & Bertout 1993, 1996; Larwood et al. 1996), radiation-driven or self-induced warping (Pringle 1996, 1997; Maloney, Begelman & Pringle 1996; Maloney & Begelman 1997; Maloney, Begelman & Nowak 1998), magnetically driven warping (Lai 1999, 2003; Pfeiffer & Lai 2004), or warping driven by frame drag-

\* E-mail: smwu@shao.ac.cn

† E-mail: lchen@shao.ac.cn, lchen@mpifr-bonn.mpg.de

‡ E-mail: fyuan@shao.ac.cn

ging (Bardeen & Petterson 1975; Kumar & Pringle 1985; Armitage & Natarajan 1999). Note also that warps generated by gravitational interactions have been investigated in the literature. In the galactic context, Hunter & Toomre (1969) studied the linear bending waves of a self-gravitating, isolated, thin disc. On nuclear disc scales, Papaloizou Terquem & Lin (1998) studied the evolution of a thin self-gravitating viscous disc interacting with a massive object orbiting the central black hole. Ulubay-Siddiki, Gerhard & Arnaboldi (2009) showed that highly warped discs near black holes can persist for a long time without any persistent forcing other than by their self-gravity. As a result, the accretion disc in some AGNs may be non-planar.

To solve the energy budget for the emission-line region for the disc model, reprocessing of the ultraviolet(UV)/X-ray continuum from the inner accretion disc is required. However, only a very small fraction of radiation from the inner disc is expected to intercept the outer part of the disc in the case of a flat geometrically thin disc. Two types of processes have been proposed to increase the fraction of light incident on the disc emission-line region. Chen, Halpern & Filippenko (1989) proposed that the inner part of the accretion disc is hot and becomes geometrically thick as a result of insufficient radiative cooling, and the X-ray emission from such an ion-supported torus is responsible for such energy input. However, double-peak emitters do not always have a low accretion rate (Zhang, Dultzin-Hacyan & Wang 2007a; Bian et al. 2007). In contrast, Cao & Wang (2006) proposed that a slow-moving jet can scatter a substantial fraction of UV/X-ray light from the inner accretion disc back to the outer part of the disc. Although this may be likely for radio-loud double-peaked emitters, the majority of double-peaked emitters are radio-quiet. In this work, we consider a system with an accretion disc around a Kerr black hole. The black hole spin is misaligned with the outer parts of the disc, as there is no physical reason to suppose that the angular momentum of the accreting mass and the angular momentum of the spinning black hole are always aligned. Frame dragging produced by a Kerr black hole causes the precession of the orbit of a particle if its orbital plane is inclined with respect to the equatorial plane of the black hole. This is known as the Lense-Thirring effect. The combined action of the Lense-Thirring effect, which tends to twist up the disc, and the internal viscosity of the accretion disc, which tends to smooth it out, forces the alignment between the angular momenta of the Kerr black hole and the accretion disc. This is known as the Bardeen-Petterson effect. This effect tends to affect the inner regions of the disc owing to the short range of the Lense-Thirring effect( $\propto r^{-3}$ ), whereas the outer part of the disc tends to keep its original inclination. The transition radius between these two regimes is known as the Bardeen-Petterson radius  $R_{BP}$  (or warp radius  $R_w$ ), and its exact location depends mainly on the physical properties of the accretion disc (Bardeen & Petterson 1975; Scheuer & Feiler 1996; Nelson & Papaloizou 2000; Fragile & Anninos 2005). Basically, the Bardeen-Petterson radius is determined by comparing the time-scale related to the Lense-Thirring precession with that of warp propagation through the disc. We consider here the propagation of warps in thin Keplerian discs in the case for which the disc is sufficiently

viscous that the warp propagates in a diffusive manner. The twisted disc itself is treated using a non-relativistic approach with an additional term describing the gravitomagnetic precession of the disc rings. Both analytic and numerical steady-state solutions have shown that the evolution of a misaligned disc arising from the Bardeen-Petterson effect usually produces an inner flat disc and a warped transition region with a smooth gradient in the tilt and twist angles (Scheuer & Feiler 1996; Natarajan & Armitage 1999; Martin, Pringle & Tout 2007). If the disc is thick and/or its viscosity is low, the warp propagates in a wave-like rather than a diffusive manner (Nelson & Papaloizou 2000; Lubow, Ogilvie & Pringle 2002). In this case, the twisted disc is not necessarily aligned with the equatorial plane at small scales. The inclination angle of a low-viscosity disc may even oscillate or counteralign close to the black hole (Lubow et al. 2002; King et al. 2005; Lodato & Pringle 2006, 2007).

The effect of a Bardeen-Petterson disc on iron line profiles treated relativistically has been examined by Fragile, Miller & Vandernoot (2005), and Bachev (1999) used a non-relativistic treatment to study the broad-line  $H\beta$  profiles from a warped disc. A relativistic treatment of the effect of a warped disc with a parametrized geometry on the Balmer lines that can be compared with observations was presented by Wu et al. (2008). Following on from these calculations, the disc warping induced by the Bardeen-Petterson effect and its influence on the broad Balmer emission owing to the reprocessing of the central high-energy radiation is investigated. In Section 2 we summarize the assumptions behind our model and present the basic equations relevant to our problem. We present our results in Section 3, and the conclusions and a discussion in Section 4.

## 2 ASSUMPTIONS AND METHOD OF CALCULATION

In this paper, we focus on how a warped disc resulting from the Bardeen-Petterson effect affects optical emission-line profiles, such as  $H\alpha$  and  $H\beta$ . A geometrically thin disc and a central ring-like illuminating source (radius denoted by  $R_r$ ) around a black hole are assumed. A short review of the basic equations relevant to our problem is given below, and readers are referred to Wu et al. (2008) for a description of our numerical scheme in more detail.

### 2.1 Geometrical considerations

The disc can be treated as being composed of a series of concentric rings of width  $dR$  and mass  $2\pi\Sigma R dR$  at radius  $R$  from the central point mass  $M$  with surface density  $\Sigma(R, t)$  at time  $t$  and with angular momentum  $\mathbf{L} = (GMR)^{1/2}\Sigma\mathbf{l} = L\mathbf{l}$ , and lying in different planes. The rings interact with each other through viscous stresses. Each ring is defined by two Eulerian angles,  $\beta(R, t)$  and  $\gamma(R, t)$ , at radius  $R$ . At each radius  $R$  from the center, the disc has a unit tilt vector  $\mathbf{l}(R, t)$  that varies continuously with radius  $R$  and time  $t$ . Following Pringle (1996), the vector  $\mathbf{l}(R, t)$  is given by

$$\mathbf{l} = (\cos \gamma \sin \beta, \sin \gamma \sin \beta, \cos \beta). \quad (1)$$

We define the normalized vector towards the observer as

$$\mathbf{i}_{obs} = (\sin i, 0, \cos i), \quad (2)$$

where  $i$  is the angle between the line of sight, and the normal to the equatorial plane lies in the XZ plane.

We define the coordinates on the surface of the disc as  $(R, \phi)$  with respect to a fixed Cartesian coordinate system  $(x, y, z)$ , where  $\phi$  is the azimuthal angle measured on the disc surface in the direction of flow, with  $\phi = \pi/2$  at the ascending node.<sup>1</sup> The element of surface area is

$$d\mathbf{S} = [\mathbf{l} + (R\beta' \cos \phi + R\gamma' \sin \beta \sin \phi) \mathbf{e}_R] R dR d\phi, \quad (3)$$

where the primes indicate differentiation with respect to  $R$ , and  $\mathbf{e}_R$  is the radial unit vector. The element of radiation flux  $dF$  received from the ring source by unit area is

$$dF \propto \frac{d\mathbf{S} \cdot \mathbf{p}}{|d\mathbf{S}|} g_r^3 I_r(\nu_r) d\Omega_r \quad (4)$$

where  $I_r(\nu_r)$  is the specific intensity measured by an observer corotating with the ring source,  $\mathbf{p}$  is the 3-momentum of an incident photon from the source,  $g_r$  is a factor to describe the shift of photon frequency along its path, which is equal to the ratio of the observed frequency from the illuminated disc to the emitted frequency from the ring source (see below).  $d\Omega_r$  is the element of the solid angle subtended by the image of the ring source observed from the illuminated disc. The Balmer lines in the illuminated surface are formed as a result of photoionization by UV/X-ray radiation from a ring-like source. For simplicity, we assume that the Balmer line intensity is proportional to the radiation being intercepted by the disc (see e.g. Fig.6a in Collin & Dumond 1989), and thus the line emissivity  $\varepsilon$  on the disc surface can take the form  $\varepsilon \propto \int dF$ . This is an approximate assumption. A detailed treatment of line emission requires solving the vertical structure as well as the radiative transfer in the disc explicitly, which is beyond the scope of this paper. We also assume that the line emission is isotropic in the comoving frame.

## 2.2 The basic equations for a warped disc

The dynamics of warping accretion discs have been discussed by a number of authors (Papaloizou & Pringle 1983; Papaloizou & Lin 1995; Demianski & Ivanov 1997; Nayakshin 2005), and the static low-viscosity configurations were first calculated by Ivanov & Illarionov (1997). This section contains a short summary of the equations describing the structure of the accretion disc models considered in this work. We follow the formalism of Pringle (1992) but add a term to describe the Lense-Thirring precession, to give

$$\begin{aligned} \dot{\Sigma} &= -\frac{1}{R}(R\Sigma V_R)' \\ \dot{\mathbf{L}} &= -\frac{1}{R}(R V_R \mathbf{L})' + \frac{1}{R} \mathbf{T}_{vis}' + \boldsymbol{\Omega}_P \times \mathbf{L} \\ \mathbf{T}_{vis} &= R^3 \Sigma (\nu_1 \Omega' \mathbf{l} + \frac{\nu_2}{2} \Omega' \mathbf{l}') \end{aligned} \quad (5)$$

(Chen, Wu & Yuan 2009). Here we use a dot to denote  $\partial/\partial t$ , and the prime symbol ( $'$ ) to denote  $\partial/\partial R$ . There are two viscosities,  $\nu_1$  and  $\nu_2$ , where  $\nu_1$  corresponds to the azimuthal shear, the standard shear viscosity in a flat disc, and  $\nu_2$  is the viscosity associated with vertical shear motions, which smoothes out the warping. The Lense-Thirring precession  $\boldsymbol{\Omega}_P$  is given by (see e.g. Kumar & Pringle 1985)  $\boldsymbol{\Omega}_P = \boldsymbol{\omega}_P/R^3$ , with:

<sup>1</sup> This definition of  $\phi$  differs by  $\pi/2$  from that of Pringle (1996).

$$\boldsymbol{\omega}_P = \frac{2G\mathbf{J}}{c^2} \quad \text{and} \quad \mathbf{J} = acM \left( \frac{GM}{c^2} \right) \mathbf{j}, \quad (6)$$

where  $\mathbf{J} = J\mathbf{j}$  is the angular momentum of the black hole.

We take both viscosities to have the same power law form, so that

$$\nu_1 = \nu_{10} \left( \frac{R}{R_0} \right)^\eta \quad \text{and} \quad \nu_2 = \nu_{20} \left( \frac{R}{R_0} \right)^\eta, \quad (7)$$

where  $\nu_{10}$ ,  $\nu_{20}$  and  $\eta$  are all constants and  $R_0$  is some fixed radius. Although the selection of  $R_0$  is in principle arbitrary, it was chosen to be the Bardeen-Petterson radius  $R_{BP}(R_w)$ , which is defined as  $\boldsymbol{\omega}_P/\nu_2$  in this work. For a steady-state warped disc, the disc shape depends only on the radius  $R_w$ . The exact value of  $R_w$  is model-dependent and is subject to some uncertainties (Natarajan & Pringle 1998; King et al. 2005; Volonteri, Sikora & Lasota 2007). To determine the value of  $R_w$ , either the Shakura & Sunyaev (1973) or the Collin & Dumond (1990) model is used. Adopting the disc properties derived by Collin & Dumond (1990), the warp radius in terms of the Schwarzschild radius of the hole,  $R_s$ , is given by (King et al. 2005)

$$\begin{aligned} \frac{R_w}{R_s} &= 990 \left( \frac{\epsilon}{0.1} \right)^{1/4} \left( \frac{L}{0.1 L_E} \right)^{-1/4} M_8^{1/8} \times \left( \frac{\alpha_1}{0.03} \right)^{1/8} \\ &\times \left( \frac{\alpha_2}{0.03} \right)^{-5/8} a^{5/8}. \end{aligned} \quad (8)$$

Here,  $\epsilon$  is the efficiency of the accretion process (i.e.  $L = \epsilon \dot{M} c^2$ ),  $L$  is the accretion luminosity,  $L_E$  is the Eddington limit,  $M_8$  is the mass of the black hole in units of  $10^8 M_\odot$ , and  $a$  is the (dimensionless) spin of the black hole.

Assuming a Shakura-Sunyaev disc (“middle region”), the warp radius can be expressed as (Volonteri et al. 2007):

$$\frac{R_w}{R_s} = 3.6 \times 10^3 a^{5/8} M_8^{1/8} \times \left( \frac{\dot{M} c^2}{L_E} \right)^{-1/4} \left( \frac{\nu_2}{\nu_1} \right)^{-5/8} \alpha_1^{-1/2}. \quad (9)$$

or, adopting the viscosity coefficient of a Shakura-Sunyaev disc as presented by Frank, King & Raine (2002), we have

$$\begin{aligned} \frac{R_w}{R_s} &= 1.41 \times 10^4 a^{4/7} \left( \frac{\nu_2}{\nu_1} \right)^{-4/7} \left( \frac{\alpha_1}{0.03} \right)^{-16/35} \left( \frac{\dot{M} c^2}{L_E} \right)^{-6/35} \\ &\times M_8^{4/35} \end{aligned} \quad (10)$$

For the typically expected standard values of AGNs,  $R_w$  is hundreds to thousands of  $R_s$ .

## 2.3 Photon motions in the background metric

We review properties of the Kerr metric and formulae for its particle orbits, and summarize here the basic equations relevant to this paper. In Boyer-Lindquist coordinates, the Kerr metric is given by (Chandrasekhar 1983):

$$ds^2 = -e^{2\nu} dt^2 + e^{2\psi} (d\phi - \omega dt)^2 + \frac{\Sigma}{\Delta} dr^2 + \Sigma d\theta^2, \quad (11)$$

where

$$e^{2\nu} = \Sigma \Delta / A, \quad e^{2\psi} = \sin^2 \theta A / \Sigma, \quad \omega = 2Mar/A,$$

$$\Sigma = r^2 + a^2 \cos^2 \theta, \quad \Delta = r^2 + a^2 - 2Mr,$$

$$A = (r^2 + a^2)^2 - a^2 \Delta \sin^2 \theta.$$

Here  $M$ ,  $a$  are the black hole mass and specific angular momentum, respectively. The equation of motion governing the orbital trajectory in the  $r\theta$ -plane is (Bardeen et al. 1972)

$$\int_{r_e}^r \frac{dr}{\sqrt{R(r)}} = \pm \int_{\theta_e}^{\theta} \frac{d\theta}{\sqrt{\Theta(\theta)}}, \quad (12)$$

where  $r_e$  and  $\theta_e$  are the starting values of  $r$  and  $\theta$ . The  $\phi$ -coordinate along the trajectory is calculated by (Wilkins 1972; Viergutz 1993)

$$\int_{\phi_e}^{\phi} d\phi = \int_{\theta_e}^{\theta} \frac{\lambda d\theta}{\sin^2 \theta \sqrt{\Theta(\theta)}} + \int_{r_e}^r \frac{(2ar - \lambda a^2) dr}{\Delta \sqrt{R(r)}}. \quad (13)$$

For photons emitted from the broad line region with radii  $>100r_g$  propagating to infinity, we can neglect terms of order  $1/r^2$  and higher in equations (12) and (13), the integral over  $\theta$  can be worked out in terms of a trigonometric integral

$$\int_{\pi/2}^{\vartheta} \frac{d\vartheta}{\sqrt{\Theta(\vartheta)}} = \frac{1}{\sqrt{\lambda^2 + q^2}} \sin^{-1}(\mu/\mu_+), \quad (14)$$

$$\int_{\pi/2}^{\vartheta} \frac{\lambda d\vartheta}{\sin^2 \vartheta \sqrt{\Theta(\vartheta)}} = \pm \sin^{-1} \sqrt{\frac{(1 - \mu_+^2)\mu^2}{\mu_+^2(1 - \mu^2)}}. \quad (15)$$

Where  $\mu = \cos \theta$  and  $0 \leq \mu < \mu_+$ ,  $\mu_+ = \sqrt{q^2/(\lambda^2 + q^2)}$ . The integral over  $r$  can be worked out using inverse Jacobian elliptic integrals (see e.g. Čadež, Fanton & Calvani 1998; Wu & Wang 2007).

The specific flux density  $F_o(\nu_o)$  at frequency  $\nu_o$  is given by (Cunningham 1975)

$$\begin{aligned} F_o(\nu_o) &= \int g^3 I_e(\nu_e) d\Omega_{\text{obs}} \\ &= \frac{q}{r_o^2 \beta \sin \vartheta_o} \int \varepsilon g^4 \delta(\nu_o - g\nu_e) \frac{\partial(\lambda, q)}{\partial(r, g)} dr dg. \end{aligned} \quad (16)$$

where  $d\Omega_{\text{obs}}$  is the element of the solid angle subtended by the image of the disc on the observer's sky and  $g$  is a factor to describe the shift of photon frequency along its path and is equal to the ratio of the observed to the emitted frequency. the emissivity  $\varepsilon$  in the integrand is calculated by

$$\varepsilon = \int \frac{d\mathbf{S} \cdot \mathbf{p}}{|d\mathbf{S}|} g_r^3 I_r(\nu_r) d\Omega_r \quad (17)$$

where  $g_r$  is the redshift for radiation between the emitter's and the observer's frame in the special case of two orbiting systems, and is given by (Viergutz 1993)

$$g_r = \frac{\gamma_d e_d \nu (1 - \Omega_d \lambda)}{\gamma_r e_r \nu (1 - \Omega_r \lambda)}, \quad (18)$$

where  $\gamma_d$  and  $\gamma_r$  are the Lorentz factor measured in the locally non-rotating frame(LNRF). The element of solid angle  $d\Omega_r$  is

$$d\Omega_r = \frac{d\alpha d\beta}{r_d^2} = \frac{1}{r_d^2} \frac{\partial(\alpha, \beta)}{\partial(\lambda, q)} \frac{\partial(\lambda, q)}{\partial(r, g_r)} dr dg_r, \quad (19)$$

where  $r_d$  is the distance from the illuminated point on the disc to the black hole. The two impact parameters  $\alpha$  and  $\beta$ , first introduced by Cunningham & Bardeen (1973), are defined as

$$\alpha = -\frac{rp^{(\varphi)}}{p^{(t)}} \quad \text{and} \quad \beta = \frac{rp^{(\theta)}}{p^{(t)}}, \quad (20)$$

where  $p^{(t)}, p^{(\theta)}, p^{(\varphi)}$  are the tetrad(or LNRF) components of the four-momentum (see e.g. Pineault & Roeder 1977; Chandrasekhar 1983).

## 2.4 Method of calculation

We now turn to how to calculate the line profiles numerically. A steady-state warped disc structure is first obtained by solving the dynamical equation numerically by setting  $\partial \mathbf{L} / \partial t = 0$  in equation (5). The disc is divided into a number of arbitrarily narrow rings, each such emitting ring being denoted by its radius  $r_i$  and weights  $\omega_i$ , provided by an algorithm developed by Rybicki G. B. (Press et al. 1992) for Gauss-Legendre integration. The main numerical procedures for computing the line profiles are as follows:

(i) Using the numerical disc structure obtained first, the values of two Eulerian angles  $\beta(R, t)$  and  $\gamma(R, t)$  at an arbitrary point are calculated by means of cubic spline interpolation.

(ii) The relevant disc system parameters are specified:  $R_{\text{in}}, R_{\text{out}}, R_r, R_w, i, \eta$  and  $\nu_2/\nu_1$ .

(iii) For a given couple  $(r_i, g)$  of a ring, the two constants of motion  $\lambda$  and  $q$  are determined if they exist.

(iv) For each  $g$ , the integration over  $r$  of equation (16) can be replaced by

$$F_o(\nu_o) = \sum_{i=1}^n \frac{q \varepsilon \nu_o^4}{r_o^2 \nu_o^4 \beta \sin \vartheta_o} \frac{\partial(\lambda, q)}{\partial(r, g)} \Big|_{r=r_i} \omega_i. \quad (21)$$

where the emissivity  $\varepsilon$  in equation (21) is calculated numerically by equation (17).

From the above formula, one can determine the line flux from the disc at an arbitrary frequency  $\nu_o$ . The observed line profile as a function of frequency  $\nu_o$  is finally obtained in this way.

## 3 RESULTS

In the accretion disc model, the double-peaked emission lines are radiated from the disc region between around several hundred gravitational radii to more than  $2000r_g$ ; here,  $r_g$  is the gravitational radius, and the widths of the double-peaked lines range from several thousand to nearly  $40,000 \text{ km s}^{-1}$  (Wang et al. 2005). In our model, all of the parameters of the warped disc are set to be free. The warp radius  $R_w$  is a key parameter for describing the disc shape. To determine the value of  $R_w$ , either the Shakura & Sunyaev (1973) or the Collin & Dumond (1990) model is used. As far as the outer region of the disc is concerned, the self-gravity of the disc must be taken into account at large radii. Beyond a certain radius, the disc becomes gravitationally unstable and can be disrupted. The typical range of unstable region is in the order of  $10^3$  to a few  $10^4$  Schwarzschild radius (Collin & Huré 1999). Thus, the reasonable range of the disc is from  $100r_g$  to  $2000r_g$ . In our calculation, the frequency ranges from 4.32 to 4.78 in units of  $10^{14} \text{ Hz}$ , and 180 bins are used. Considering the broadening arising from electron scattering or turbulence, all our results are smoothed by convolution with a  $3\sigma$  Gaussian.

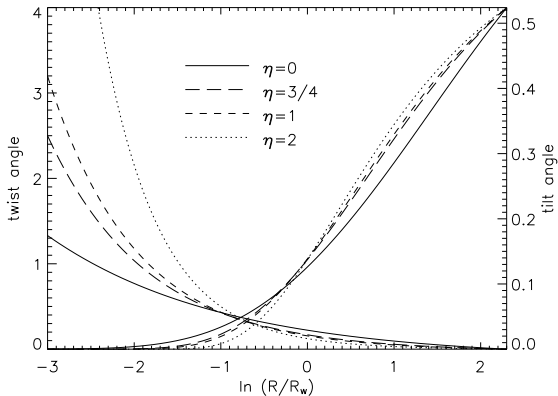


**Figure 1.** The distribution of  $\beta$  and  $\gamma$  as a function of radius. The twist angle  $\gamma$  is measured in units of  $2\pi$ , and the tilt angle  $\beta$  is shown in radians. The solid, long-dashed, short-dashed and dotted lines show the results for  $\eta = 0, 3/4, 1$  and  $2$ , respectively.

### 3.1 The numerical steady-state warped disc solutions

We numerically solved equation (5), setting all the time differentials to zero, in order to find a steady-state disc structure. As a boundary condition, we set  $\beta = \pi/6$  and  $\gamma = 0$  at the outer boundary. The calculation region is  $-4.6 < x < 2.3$ , where  $x = \ln(R/R_w)$ , or, equivalently,  $R_{in} = R_w e^{-4.6} \approx 0.01 R_w$ , and  $R_{out} = R_w e^{2.3} \approx 10 R_w$ . The calculated distributions of  $\beta$  and  $\gamma$  as a function of radius are plotted in Fig. 1.

### 3.2 Line profiles from twisted warping discs

We use the numerical code developed by Wu et al. (2008) to evaluate the line profiles for the numerical disc structure obtained. We first calculated the line profiles of a simplified model with no relativistic effects included in equations of propagation of photons and compared them with the relativistic treatment. The parameters of the two Eulerian angles and the disc range are identical to those found by Bachev (1999), but we used a ring-like primary source and a linear response for the reprocessing to the ionizing flux. The primary source radius is set to  $R_r = 1.5 r_g$ . We reproduced the results obtained by Bachev (1999) on a qualitative level. A comparison between the  $H\beta$  line profiles for a simplified model with no relativistic effects (solid line) and those with the relativistic treatment (dotted line) is shown in Fig. 2. The influence of the gravitational lensing, which concentrates the radiation from the innermost region towards the equatorial plane on the line profile, is significant.

The dependence of the  $H\alpha$  line profiles on the primary source radius  $R_r$  is plotted in Fig. 3. The radii with respect to the different lines are:  $R_r = 1.5 r_g$  (solid line),  $2.0 r_g$  (dotted line),  $3.0 r_g$  (short-dashed line),  $6.0 r_g$  (dot-dashed line),  $10.0 r_g$  (long-dashed line). The other parameters are  $R_{in} = 150 r_g$ ,  $R_{out} = 1200 r_g$ ,  $R_w = 600 r_g$ ,  $\eta = 1$ ,  $\nu_2/\nu_1 = 10$  and  $i = 30^\circ$ . The azimuthal viewing angle along the XY-plane varies from  $0^\circ$  to  $300^\circ$  in steps of  $60^\circ$  from the top left-hand to the bottom right-hand panel. The vertical

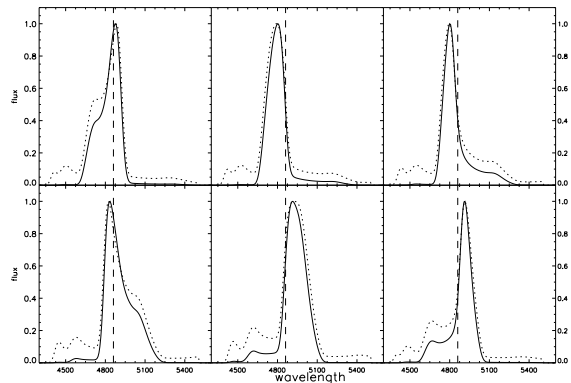


**Figure 2.** Comparison of the  $H\beta$  line profiles between a simplified model with no relativistic effects (solid line) and one with the relativistic treatment (dotted line). The parameters of two Eulerian angles and the disc range are identical to those presented by Bachev (1999). The azimuthal viewing angle along the XY-plane varies from  $0^\circ$  to  $300^\circ$  in steps of  $60^\circ$  from the top left-hand panel to the bottom right-hand panel. The vertical dashed line corresponds to the wavelength position of  $H\beta$  in the rest frame.

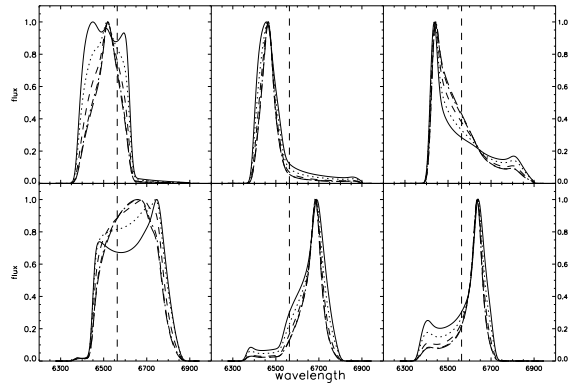


**Figure 3.** Comparison of the  $H\alpha$  line profiles with different primary source radii  $R_s$ :  $R_s = 1.5 r_g$  (solid line),  $2.0 r_g$  (dotted line),  $3.0 r_g$  (short dashed line),  $6.0 r_g$  (dot-dashed line),  $10.0 r_g$  (long dashed line). The other parameters are  $R_{in} = 150 r_g$ ,  $R_{out} = 1200 r_g$ ,  $R_w = 600 r_g$ ,  $\eta = 1$ ,  $\nu_2/\nu_1 = 10$  and  $i = 30^\circ$ . The azimuthal viewing angle along the XY-plane varies from  $0^\circ$  to  $300^\circ$  in steps of  $60^\circ$  from top left-hand panel to bottom right-hand panel. The vertical dashed line corresponds to the wavelength position of  $H\alpha$  in the rest frame.

dashed line corresponds to the wavelength position of  $H\alpha$  in the rest frame. From this figure, it can be seen that the line profiles are not sensitive to a change in the radius of the primary source in the range from  $3.0 r_g$  to  $10.0 r_g$ , but that they have a significant dependence when it approaches the innermost stable orbit.

The images of the illuminated area and the  $H\alpha$  line profiles computed by our code for a steady-state twisted warped disc are shown in Fig. 4. The disc zone is from  $R_{in} = 150 r_g$  to  $R_{out} = 1200 r_g$ , the warp radius is set to  $R_w =$

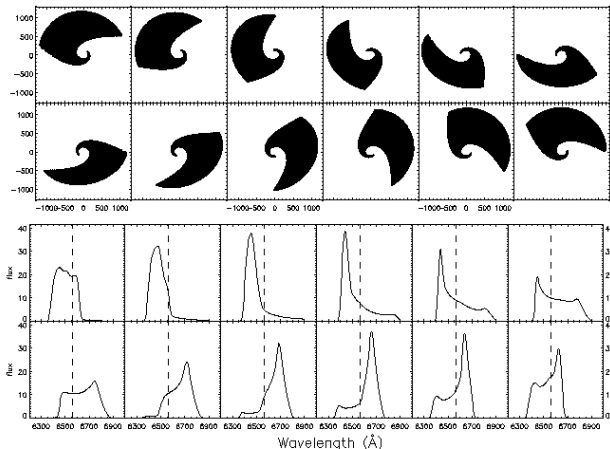


**Figure 4.** Images (upper panels) of the illuminated area of the disc and the  $H\alpha$  line profiles (lower panels) computed by our code for the twisted warped disc case for  $i = 30^\circ$ ; the disc zone is from  $R_{\text{in}} = 150r_g$  to  $R_{\text{out}} = 1200r_g$ . The Bardeen-Petterson radius is set to  $R_w = 600r_g$ ,  $\eta = 3/4$  and  $\nu_2/\nu_1 = 10$ . The azimuthal viewing angle along the XY-plane varies from  $0^\circ$  to  $330^\circ$  in steps of  $30^\circ$  from the top left-hand panel to the bottom right-hand panel.

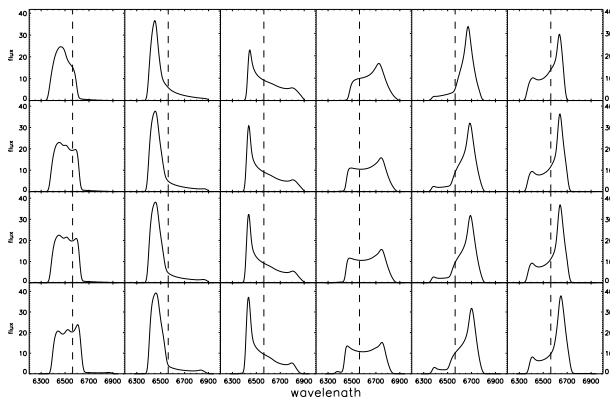


**Figure 5.** Comparison of the  $H\alpha$  line profiles for a warped disc with various values of the power-law index of the viscosity:  $\eta = 0, 3/4, 1, 2$  (from top to bottom rows). The other parameters are  $i = 30^\circ$ ,  $R_{\text{in}} = 150r_g$ ,  $R_{\text{out}} = 1200r_g$  and  $R_w = 600r_g$ . The azimuthal viewing angle along the XY-plane varies from  $0^\circ$  to  $300^\circ$  in steps of  $60^\circ$  (from the left- to the right-hand side).

$600r_g$ , and the other parameters are  $i = 30^\circ$ ,  $\eta = 3/4$  and  $\nu_2/\nu_1 = 10$ . The azimuthal viewing angle along the XY-plane varies from  $0^\circ$  to  $330^\circ$  in steps of  $30^\circ$  from the top left-hand to the bottom right-hand panel. The image contains  $400 \times 360$  pixels. From the images, we can see that, moving inwards from the outer radius of the disc, the warp is twisted by an angle of  $\sim \pi$  before being flattened efficiently into the aligned plane, as is also shown in Fig. 1.

The influence of the power-law index of the viscosity on the line profiles for  $\eta = 0, 3/4, 1, 2$  (from top to bottom panels) is shown in Fig. 5. The disc zone is from  $R_{\text{in}} = 150r_g$  to  $R_{\text{out}} = 1200r_g$ ; the other parameters are  $i = 30^\circ$ ,

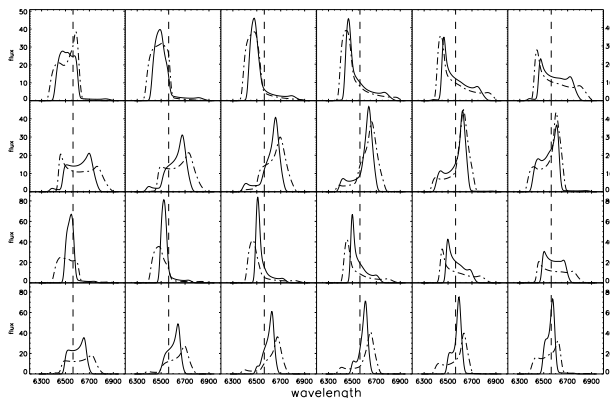


**Figure 6.** Comparison of the  $H\alpha$  line profiles with various values of the Bardeen-Petterson radius or viewing angle. Upper two rows: the parameters are  $i = 30^\circ$ ,  $R_{\text{in}} = 150r_g$ ,  $R_{\text{out}} = 2000r_g$ ,  $\eta = 3/4$ ,  $\nu_2/\nu_1 = 10$  and  $R_w = 1000r_g$  (solid line),  $R_w = 500r_g$  (dot-dashed line). Lower two rows: the parameters are  $R_{\text{in}} = 150r_g$ ,  $R_{\text{out}} = 1500r_g$ ,  $R_w = 800r_g$ ,  $\eta = 1$ ,  $\nu_2/\nu_1 = 10$  and  $i = 15^\circ$  (solid line),  $i = 30^\circ$  (dot-dashed line). The azimuthal angle along the XY-plane varies from  $0^\circ$  to  $330^\circ$  in steps of  $30^\circ$  from the top left-hand to the bottom right-hand panel.

$R_w = 600r_g$ . The azimuthal viewing angle along the XY-plane varies from  $0^\circ$  to  $300^\circ$  in steps of  $60^\circ$  (from the left- to the right-hand side). The general behaviour of the line profile is similar. Fig. 6 shows the dependence of the profiles on the warp radius and viewing angle. The upper panels are for  $i = 30^\circ$ ,  $R_{\text{in}} = 150r_g$ ,  $R_{\text{out}} = 2000r_g$ ,  $\eta = 3/4$ ,  $\nu_2/\nu_1 = 10$  and  $R_w = 1000r_g$  (solid line),  $R_w = 500r_g$  (dot-dashed line). The lower panels show the profile dependence on the viewing angles for  $i = 15^\circ$  (solid line) and  $i = 30^\circ$  (dot-dashed line). The other parameters are  $R_{\text{in}} = 150r_g$ ,  $R_{\text{out}} = 1500r_g$ ,  $R_w = 800r_g$ ,  $\eta = 1$  and  $\nu_2/\nu_1 = 10$ .

Generally speaking, the profiles of the line emission from the warped disc induced by the Bardeen-Petterson effect are nonsymmetrical and red- or blue-frequency-shifted in most cases for which the primary source radius is large. When the primary source radius approaches the innermost stable orbit, double-peaked or triplet-peaked line profiles are present in most cases. Thus, a warped disc induced by the Bardeen-Petterson effect provides a mechanism for producing the double- or triplet-peaked line profiles that were observed in the Sloan Digital Sky Survey. The triplet-peaked line profile, such as for SDSS J084205.57+075925.5 and SDSS J232721.96+152437.3 (see e.g. Wu et al. 2008), may be a “signature” of a warped disc. Future monitoring of line profile variability in these triplet sources will provide a critical test of the warped disc model.

## 4 SUMMARY

We computed the Balmer emission-line profiles that result from the reprocessing of emission using a numerical model of a warped disc induced by the Bardeen-Petterson effect, including all relativistic effects for radiation propagation, and subject to various shadowing effects associated with disc warping. We numerically solved the disc structure for

a steady-state disc shape. To simplify the analysis, we took both viscosities to have the same power-law form, and thus the ratio  $\nu_2/\nu_1$  is independent of radius. For simplicity, we assumed that the disc is illuminated by a ring-like central source, which is a rough approximation, that the line emissivity is proportional to the continuum light intercepted by the accretion disc, and that line emission is isotropic. Our conclusions are as follows.

(i) From the numerical results, we can see that, moving inwards from the outer radius of the disc, the warp is twisted by an angle of  $\sim \pi$  before being flattened efficiently into the equatorial plane.

(ii) For a given warped disc, there are two angles that determine the observed line profile, the inclination angle and the azimuthal viewing angle resulting from the non-axisymmetry of the disc warping.

(iii) For less twisted warped disc induced by the Bardeen-Petterson effect, the asymmetrical and frequency-shifted single-peaked line profiles are produced in most cases when the primary source radius is large (from  $3r_g$  to  $10r_g$ ). The double- or triplet-peaked line profiles presented in most cases occur when the primary source radius approaches the marginally stable orbit of an extreme Kerr black hole.

The line profiles depend strongly on the twisting structure of the disc (Wu et al. 2008) as well as on the radius of the illuminating source. The Doppler effect and gravitational focusing concentrate the radiation from the innermost region towards the equatorial plane, which increases the returning flux (Cunningham 1975, 1976). This may be the reason why the illuminating source radius has a strong influence on the line profile. Knowledge of the twisting structure may allow the determination of some important characteristics of AGNs, such as the spin of the black hole and the viscosities of the disc. We assume that the ratio  $\nu_2/\nu_1$  is independent of radius in the calculations, but the relation between  $\nu_1$  and  $\nu_2$  is very uncertain, and may influence the disc twisting structure. It is also important to emphasize that, although we have analyzed the Bardeen-Petterson effect in this work, the four mechanisms mentioned above are not mutually exclusive. This means that more than one mechanism might be operating in a given system.

## 5 ACKNOWLEDGMENTS

We would like to thank the anonymous referee for helpful suggestions and comments, which improved and clarified our paper. This work was supported in part by the Natural Science Foundation of China (grants 10773024, 10833002, 10821302, and 10825314), Bairen Program of Chinese Academy of Sciences, and the National Basic Research Program of China (973 Program 2009CB824800).

## REFERENCES

Armitage P. J., Natarajan P. 1999, *ApJ*, 525, 909  
 Bardeen J. M., Petterson J. A. 1975, *ApJ*, 195, L65  
 Bardeen J. M., Press W. H., Teukolsky S. A., 1972, *ApJ*, 178, 347  
 Bachev R., 1999, *A&A*, 348, 71

Begelman M. C., Blandford R. D., Rees M. J., 1980, *Nature*, 287, 307  
 Bian W.-H., Chen Y.-M., Gu Q.-S., Wang J.-M., 2007, *ApJ*, 668, 721  
 Čadež A., Fanton C., Calvani M., 1998, *New Astronomy*, 3, 647  
 Cao X., Wang T. G., 2006, *ApJ*, 652, 112  
 Caproni A., Abraham Z., Mosquera Cuesta H. J., 2006, *ApJ*, 638, 120  
 Caproni A., Abraham Z. Livio M., Mosquera Cuesta H. J., 2007, *MNRAS*, 379, 135  
 Chakrabarti S., Wiita P. J., 1994, *ApJ*, 434, 518  
 Chandrasekhar S., 1983, *The Mathematical Theory of Black Holes*, Oxford Univ. Press, NY  
 Chen K., Halpern J. P., Filippenko A. V., 1989, *ApJ*, 339, 742  
 Chen L, Wu S.-M., Yuan F., 2009, *MNRAS*, 398, 1900  
 Collin-Souffrin S., Dumond A. M., 1989, *A&A*, 213, 29  
 Collin-Souffrin S., Dumond A. M., 1990, *A&A*, 229, 292  
 Collin-Souffrin S., Huré J. M., 1999, *A&A*, 342, 385  
 Cunningham C. T., 1975, *ApJ*, 202, 788  
 Cunningham C. T., 1976, *ApJ*, 208, 534  
 Cunningham C. T., Bardeen J. M., 1973, *ApJ*, 183, 237  
 Demianski M., Ivanov P.B., 1997, *A&A*, 324, 829  
 Eracleous M., Halpern J. P., 1994, *ApJS*, 90, 1  
 Eracleous M., Halpern J. P., 2003, 599, 886  
 Eracleous M., Livio M., Halpern J. P., Storchi-Bergmann T., 1995, *ApJ*, 438, 610  
 Fragile P. C., Anninos P., 2005, *ApJ*, 623, 347  
 Fragile P. C., Miller W. A., Vandernoot E., 2005, *ApJ*, 635, 157  
 Frank J., King A., Raine D., 2002, *Accretion Power in Astrophysics*, Cambridge Univ. Press, NY  
 Gezari S., Halpern J. P., Eracleous M., 2007, *ApJS*, 169, 167  
 Gaskell C. M., 1996, *ApJ*, 464, 107  
 Herrnstein J. R., Moran J. M., Greenhill L. J., Trotter A., 2005, *ApJ*, 629, 719  
 Hunter C., Toomre A., 1969, *ApJ*, 155, 747  
 Ivanov P.B., Illarionov A.F., 1997, *MNRAS*, 285, 394  
 Kumar S., Pringle J. E., 1985, *MNRAS*, 213, 435  
 King A. R., Lubow S. H., Ogilvie G. I., Pringle J. E., 2005, *MNRAS*, 363, 49  
 Lai D. 1999, *ApJ*, 524, 1030  
 Lai D. 2003, *ApJ*, 591, L119  
 Larwood J. D., Nelson R. P., Papaloizou J. C. B., Terquem C., 1996, *MNRAS*, 282, 597  
 Lodato G., Pringle J. E., 2006, *MNRAS*, 368, 1196  
 Lodato G., Pringle J. E., 2007, *MNRAS*, 381, 1287  
 Lubow S. H., Ogilvie G. I., Pringle J. E., 2002, *MNRAS*, 337, 706  
 Maloney P. R., Begelman M. C., Pringle J. E., 1996, *ApJ*, 472, 582  
 Maloney P. R., Begelman M. C., 1997, *ApJ*, 491, L43  
 Maloney P. R., Begelman M. C., Nowak M. A., 1998, *ApJ*, 504, 77  
 Martin R. G., Pringle J. E., Tout C. A., 2007, *MNRAS*, 381, 1617  
 Martin R. G., Tout C. A., Pringle J. E., 2008, *MNRAS*, 387, 188  
 Miller J. S., Peterson B. M., 1990, *ApJ*, 361, 98  
 Natarajan P., Pringle J. E., 1998, *ApJ*, 506, L97

- Natarajan P., Armitage P. J., 1999, MNRAS, 309, 961  
Nayakshin S. , 2005, MNRAS, 359, 545  
Nelson R. P., Papaloizou J. C. B., 2000, MNRAS, 315, 570  
Papaloizou J. C. B., Pringle J. E., 1983, MNRAS, 202, 1181  
Papaloizou J.C.B., Lin D.N.C., 1995, ApJ, 438, 841  
Papaloizou J.C.B., Terquem C., Lin D.N.C., 1998, ApJ, 497, 212  
Pfeiffer H. P., Lai D., 2004, ApJ, 604, 766  
Pineault S., Roeder R. C., 1977, ApJ, 213, 548  
Press W. H., Teukolsky S. A., Vetterling W. T., Flannery B. P., 1992, Numerical Recipes. Cambridge University Press, Cambridge  
Pringle J. E., 1992, MNRAS, 258, 811  
Pringle J. E., 1996, MNRAS, 281, 357  
Pringle J. E., 1997, MNRAS, 292, 136  
Scheuer P. A. G., Feiler R., 1996, MNRAS, 282, 291  
Shakura N. I., Sunyaev R. A., 1973, A&A, 24, 337  
Storchi-Bergmann T. , Eracleous M., Ruiz M. T. , Livio M. , Wilson A. S. , Filippenko A. V., 1997, ApJ, 489, 87  
Strateva I. V. et al., 2003, AJ, 126, 1720  
Terquem C., Bertout C., 1993, A&A, 274, 291  
Terquem C., Bertout C., 1996, MNRAS, 279, 415  
Ulubay-Siddiki A., Gerhard O., Arnaboldi M., 2009, MNRAS, 398, 535  
Veilleux S., Zheng W., 1991, ApJ, 377, 89  
Viergutz S. U., 1993, A&A, 272, 355  
Volonteri M., Sikora M., Lasota J.-P., 2007, ApJ, 667, 704  
Wang T.-G., Dong X.-B., Zhang X.-G., Zhou H.-Y., Wang J.-X., Lu Y.-J, 2005, ApJ, 625, L35  
Wu S.-M., Wang T.-G., 2007, MNRAS, 378, 841  
Wu S.-M., Wang T.-G., Dong X.-B., 2008, MNRAS, 389, 213  
Wilkins D. C., 1972, Phys. Rev. D5, 814  
Zhang X. -G., Dultzin-Hacyan D., Wang T.-G., 2007a, MNRAS, 376, 1335  
Zhang X. -G., Dultzin-Hacyan D., Wang T.-G., 2007b, MNRAS, 377, 1215  
Zheng W., Sulentic J. W., Binette L., 1990, ApJ, 365, 115